Structural Effects on the Spin Dynamics of Potential Molecular Qubits

Structural Effects on the Spin Dynamics of Potential Molecular Qubits

Matteo Atzori,[†] Stefano Benci,[‖] Elena Morra,[‡] Lorenzo Tesi,[†] Mario Chiesa,[‡] Renato Torre,[‖,§] Lorenzo Sorace,[†] and Roberta Sessoli[†]

[†] Dipartimento di Chimica "Ugo Schiff" e INSTM, Università degli Studi di Firenze, Via della Lastruccia 3, I50019 Sesto Fiorentino (Firenze), Italy.

[‖] European Lab. for Non-Linear Spectroscopy, Università degli Studi di Firenze, I50019 Sesto Fiorentino (Firenze), Italy.

[§] Dipartimento di Fisica ed Astronomia, Università degli Studi di Firenze, I50019 Sesto Fiorentino (Firenze), Italy.

[‡] Dipartimento di Chimica e NIS Centre, Università di Torino, Via P. Giuria 7, I10125 Torino, Italy.

ABSTRACT: To observe long quantum coherence in spin systems, control of spin-lattice relaxation is crucial. Such a control is most often extremely difficult to achieve because of the simultaneous presence of competitive relaxation mechanisms - *direct, Raman, Orbach* - not always easily relatable to the calculated energy states of the investigated system due to the involvement of additional spin-phonon coupling phenomena to the relaxation, such as spin-vibration coupling mediated by intramolecular vibrations. In this work we have investigated the effect of slight changes on the molecular structure of four vanadium(IV)-based potential spin qubits on their spin dynamic studied by alternate current (AC) susceptometry. The analysis of the magnetic field dependence of the relaxation time well correlates with the low energy vibrational modes experimentally detected by time-domain THz spectroscopy, thus confirming and extending our preliminary observations on the role played by spin-vibration coupling in determining the fine-structure of the spin-lattice relaxation time as a function of the magnetic field for $S = ½$ potential spin qubits. This study represents a step forward the use of low energy vibrational spectroscopy as a prediction tool for the design of molecular spin qubits with long-lived quantum coherence. Indeed, a quantum coherence time of ca. 4.0 μs in the 4–100 K range is observed for the most performing vanadyl derivative identified through this multitechnique approach.

INTRODUCTION

In the last few years, great interest has been devoted to the experimental implementation of quantum information, one of the pillars of the technological revolution that is foreseen for the next decades. Quantum information has its core in the quantum bit, or qubit, *i.e.* a two levels quantum-mechanical system able to be placed in a state of coherent superposition.[1] Qubits implementation requires the accomplishment of stringent and somehow conflicting prerequisites known as DiVincenzo criteria,[2] and the preparation and investigation of viable qubits represents a challenging current research task. Several systems can be used as qubits, such as photons,[3] ionic traps,[4] superconducting circuits,[5] and spins.[6,7] Spin systems are particularly advantageous from an application point of view because they can be easily manipulated through external magnetic[8] and electric fields,[9] such as electron paramagnetic resonance (EPR) techniques.

Spin qubits can be either nuclear or electronic, and nowadays, the most investigated are nitrogen-vacancy pairs in diamond[10,11] or defects in silicon[6] or silicon carbide.[12] On the contrary, electronic spin systems based on paramagnetic metal ions in coordination complexes[13,14] are, to date, less investigated even if they show higher tunability than purely inorganic systems. Indeed, the electronic spin in molecular systems can be finely controlled by playing with the coordination geometries and the bonded ligands.[7,15,16,17,18]

Despite the advantages related to their chemical tunability, molecular systems still show shorter lifetimes of the quantum superposition of states, which is a key parameter to evaluate their potential application for quantum logic operations.[1] The lifetime of the superposition state is determined by the spin-spin relaxation time T_2, and it is usually quantified by the phase memory time T_m, which is a measurable lower limit of T_2. Remarkably, mononuclear vanadium(IV) complexes with nuclear spin-free ligands can attain at low temperature a T_m of the order of a millisecond when dispersed in a nuclear spin-free solvent such as CS_2,[19] a value comparable to those observed for electronic defects in extended lattices. Another fundamental parameter to evaluate the spin qubit performances is the spin-lattice relaxation time T_1, which represents the time required to an excited spin to relax back to its ground state. Control of T_1 is of crucial importance; if too long it limits the speed of initialization of the qubit, while if too short it induces a collapse of T_2, especially as the temperature increases.[20]

Control of spin-lattice relaxation in molecular systems, either spin qubits or single-molecule magnets (SMMs),[21] is very difficult to achieve as a consequence of different types

of relaxation mechanisms that can be potentially involved, that is *direct*, *Raman*, and *Orbach*, all of them related to different and specific energy states of the system and its surrounding lattice. Restricting the discussion to the class of molecular spin qubits based on $S = ½$ spin states, where the Orbach mechanism of relaxation cannot be observed due to the lack of available magnetic states besides the $m_S = \pm½$ doublet, the temperature dependence of the spin-lattice relaxation is mainly determined by the direct and the Raman mechanisms.

In a recent investigation we have suggested that the magnetic field dependence of the spin-lattice relaxation time in potential qubits based on the $S = ½$ spin of the V^{IV} ion, is not simply determined by the combination of direct and Raman mechanisms of relaxation, but is also affected by relaxation mechanisms which involve low energy vibrational modes.[22] Intramolecular vibrational modes were identified as one of the ways for the magnetization to relax back to the ground state, but the study concerning the correlation between the energy of the involved phonons and the spin-lattice relaxation time is still in its infancy. On this regard, a few recently published studies have highlighted that the chemical control of local vibrations can be a winning strategy to design functional spin qubits[23] or SMMs[24,25] that can operate at higher temperatures.

Herein we report the investigation of the magnetization dynamics of four vanadium(IV)-based complexes performed to understand the role played by the molecular structure of highly coherent spin qubits on their spin dynamics *via* spin-vibration coupling. To study the correlation between the local structural parameters and the behaviour of the spin-lattice relaxation time as a function of the magnetic field, specific changes in their molecular structures have been introduced. More specifically, the rigidity of the coordination sphere was modified by synthesizing tris-chelated octahedral and vanadyl square-pyramidal complexes of the same ligand, while the ligand rigidity was modified by increasing the number of condensed aromatic rings. We have then identified and prepared two vanadyl complexes with catecholate (cat) and naphthalene-catecholate (naph-cat) ligands, namely $[(Ph)_4P]_2[VO(cat)_2]$ (**1**) and $[(Ph)_4P]_2[VO(naphcat)_2]$ (**3**), and their respective tris-chelated octahedral complexes of the bare V^{IV} ion, namely $[(Ph)_4P]_2[V(cat)_3]$ (**2**) and $[(Ph)_4P]_2[V(naph\text{-}cat)_3]$ (**4**). We have thus investigated *i)* the magnetic relaxation as a function of the temperature and the applied magnetic field by AC susceptibility measurements, *ii)* the low energy vibrational modes for the four systems by time-domain THz spectroscopy, and *iii)* the quantum coherence time as a function of the temperature of the best performing system identified by the combination of the above-mentioned techniques through pulsed EPR spectroscopy experiments.

The differences on the spin dynamics of the four selected systems are discussed on the basis of the two main structural modifications introduced, *i.e. i)* the change in the coordination geometry, and *ii)* the different molecular structure of the coordinating ligands, revealing important insights on the role of chemical design to improve the performances of potential molecular spin qubits or SMMs.

RESULTS AND DISCUSSION

Synthesis. Catechol has an exceptional chelating ability. In aqueous media it is able to displace the oxygen of the vanadyl ion to generate the tris-chelated octahedral coordination complexes of the bare V^{IV} ion.[26] Consequently, reaction of catecholate or naphthalene-catecholate with vanadyl(IV) sulfate easily provides the octahedral coordination complexes **2** and **4** (Scheme 1b). The preparation of the square pyramidal complexes of the vanadyl ion can instead be achieved by working in strongly basic solution. Indeed, the presence of an extra content of base forces the $[VO(L)_2]^{2-} + HL^- \rightleftarrows [V(L)_3]^{2-} + OH^-$ (L = cat or naph-cat) equilibrium toward the formation of the $[VO(L)_2]^{2-}$ species[26], **1** and **3** in this work (Scheme 1a).

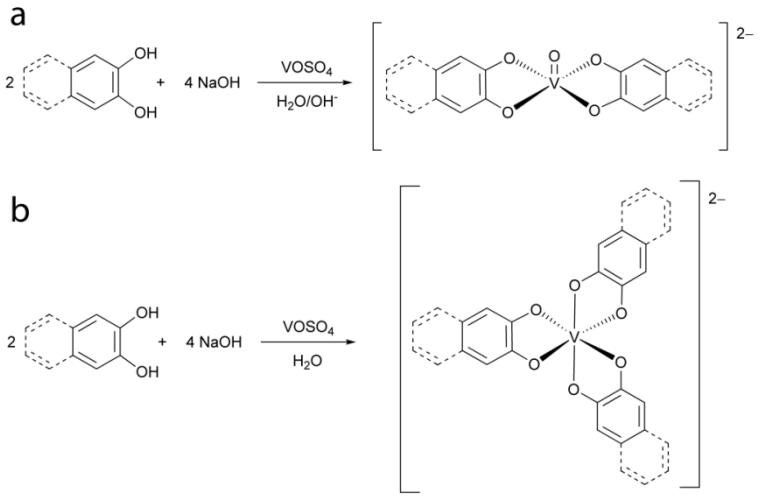

Scheme 1. Reaction schemes for the synthesis of **1** and **3** (a), and **2** and **4** (b).

Crystal Structures. Single crystals suitable for X-ray diffraction analysis of compound **1** were obtained by recrystallization from acetone of the crude product obtained from aqueous media. Compound **1** crystallizes in the monoclinic $P2_1/c$ space group with one anionic complex and two tetraphenylphosphonium counterions in the asymmetric unit. Its crystal structure consists of symmetry related $[VO(cat)_2]^{2-}$ anions separated by

tetraphenylphosphonium counterions (Figure S1). The complex anions are fully surrounded by tetraphenylphosphonium counterions (Figure S2), thus any intramolecular contacts shorter than the sum of the van der Waals radii between metal complexes is precluded. As a result, the shortest M···M distance in the crystal structure of **1** is 11.95 Å.

The molecular structure of the dianionic complex of **1** is shown in Figure 1a. It presents a slightly distorted square pyramidal coordination geometry due to the chelating ligand, with the metal ions slightly above the basal plane (ca. 0.62 Å) formed by the four oxygen donor atoms. The apical position is occupied by an oxo ligand which forms a double bond with the V^{IV} ion, with a resulting V=O bond distance of 1.614 Å, whereas the V − O single bond lengths are in the 1.960–1.980 Å range. These structural findings well match with those previously reported of the same anionic complex having K^+ as counterion.[26]

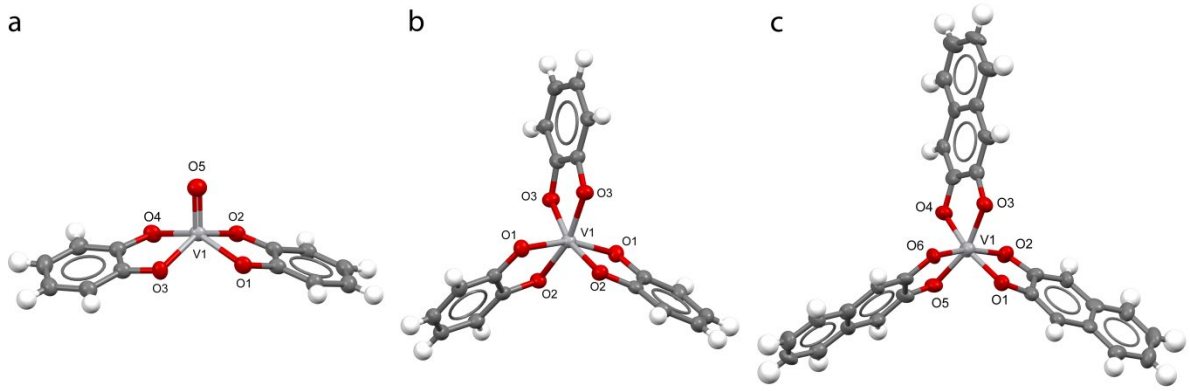

Figure 1. Molecular structure of the dianionic complexes of compounds **1** (a), **2** (b), and **4** (c) with principal atoms labelling scheme.

Single crystals suitable for X-ray diffraction analysis of compounds **2** and **4** were obtained by slow evaporation of CH_2Cl_2 solutions. Compound **2** crystallizes in the monoclinic *C2/c* space group with half anionic complex and one tetraphenylphosphonium in the asymmetric unit, while compound **4** crystallizes in the monoclinic $P2_1/n$ space group with one anionic complex and two tetraphenylphosphonium counterions in the asymmetric unit. The crystal structures of **2** and **4** consist of homoleptic tris-chelated $[V(cat)_3]^{2-}$ or $[V(naph\text{-}cat)_3]^{2-}$ anions showing Λ and Δ chirality and tetraphenylphosphonium cations (Figure S3). The shortest M···M distance is 10.12 Å for **2** and 14.30 Å for **4**. The longer distance observed for the latter is clearly due to the presence of a bulkier coordinating ligand. Also in these cases, contacts shorter than the sum of the van der Waals radii between metal complexes are completely precluded by the presence of the counterions, whereas the C–H···π and C–H···H

interactions between the counterions and the catecholate ligands of each metal complex dominate.

The molecular structures of the complex anions of **2** and **4** are reported in Figure 1b-1c. The coordination geometry around the V^{IV} ion is a distorted octahedron with an average V–O distance of 1.946 Å and 1.941 Å for **2** and **4**, respectively. These structural findings are in agreement with those previously reported for the tris-chelated complex of V(IV) with catecholate as ligand and triethylammonium as counterion,[26] while no structural data have been reported so far for octahedral complexes of V^{IV} with naph-cat as ligand.

In all structurally characterized compounds the intraligand bond distances are in the usual range for the dianionic coordinated catecholate moiety (Table S1), thus excluding any evidence for the quinone or semiquinone forms of the ligand.

All attempts to crystallize **3** were unsuccessful because of its tendency to slowly convert in solution into the tris-chelated complex **4** during the crystallization processes. However, single crystal structural data already reported in the literature for the same anionic complex, $[VO(naph\text{-}cat)]^{2-}$, with a different counterion, namely trimetylenediammonium,[27] provides a V=O bond length of 1.604 Å, and V–O single bond lengths in the 1.927–1.975 Å range, that well compare to those observed for **1**.

Continuous Wave Electron Paramagnetic Resonance Spectroscopy. CW EPR spectra on frozen solution were recorded to have a full description of the electronic properties of compounds **1**–**4**. The spectra recorded at 50 K for **1** and **2** are reported in Figure 2 together with their simulations, while those of **3** and **4** are reported in Figure S4.

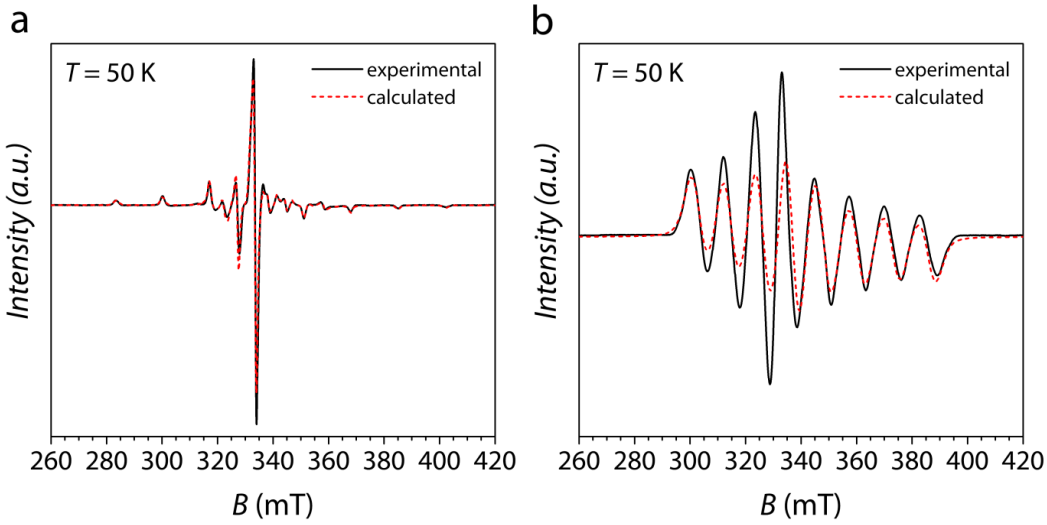

Figure 2. Experimental and simulated (see legend) CW EPR on frozen solution (1.0 mM in CH_2Cl_2:C_6H_6 3:1) spectra for **1** (a) and **2** (b) at X-band frequency (9.3 GHz).

As expected, the EPR spectra show the eight-fold hyperfine splitting due to the nuclear-spin coupling between the $S = 1/2$ electronic spin of V^{IV} and the $I = 7/2$ nuclear spin of its most abundant isotope (^{51}V, abundance 99.76%). The signal of **1** is further split by the anisotropic components of the hyperfine coupling in perpendicular and parallel directions (Figure 2a), while the spectrum of **2** shows very broad absorption lines, which do not allow a simple visual assignment of the hyperfine transitions (Figure 2b). Spectral simulations[28] were then performed on the basis of the following spin Hamiltonian

$$\mathcal{H} = \hat{\boldsymbol{I}} \cdot \boldsymbol{A} \cdot \hat{\boldsymbol{S}} + \mu_B \hat{\boldsymbol{S}} \cdot \boldsymbol{g} \cdot \boldsymbol{B} \qquad (3)$$

to evaluate the anisotropy of the $\boldsymbol{g}$ factor as well as that of the hyperfine coupling constant $\boldsymbol{A}$ for all complexes. The spectra can be satisfactorily simulated assuming a rhombic model (*i.e.* $x \neq y \neq z$) for **1**, **3** and **4**, and an axial model (*i.e.* $x = y \neq z$) for **2**. The best-fit parameters are reported in Table 1.

Table 1. Best-fit parameters extracted from simulation of the experimental spectra of **1-4**.

Compound	g_x	g_y	g_z	$\lvert A_x \rvert$ (MHz)	$\lvert A_y \rvert$ (MHz)	$\lvert A_z \rvert$ (MHz)
1	1.980(1)	1.988(1)	1.956(1)	159(2)	126(2)	465(2)
2	1.947(1)	1.947(1)	1.971(1)	330(2)	330(2)	60(2)
3	1.979(1)	1.988(1)	1.955(1)	156(2)	127(2)	465(2)
4	1.914(1)	1.926(1)	2.003(1)	393(2)	241(2)	27(2)

The data reported in Table 1 indicates that the presence of a short V=O bond in **1** and **3** is responsible for a *d*-orbitals splitting of the metal centres that leaves the d_{xy} orbital lowest in energy with respect to the other orbitals, as expected. On the contrary, the octahedral coordination geometry of **2** and **4** is responsible for a *d*-orbital splitting that leaves the d_z^2 orbital lowest in energy with respect to the other orbitals. This feature, together with a single unpaired electron of the $S = 1/2$ V^{IV} ion, makes such compounds suitable two level states potential molecular qubits. However, although both ligand field symmetries provide a well isolated doublet ground state, it has been recently suggested that the weaker angular orbital momentum contribution to the ground state in vanadyl complexes with respect to the octahedral vanadium(IV) ones dramatically influence the magnitude of the observed relaxation times, which are in general higher for the oxovanadium(IV) complexes.[20]

It is worth noting that the structural modification introduced by extending the ligand structure induces only very minor modification on the Spin Hamiltonian parameters of the

metal center for **1** and **3**, suggesting that the key structural feature for these systems is the rigidity of the coordination geometry imposed by the V=O bond. On the contrary, higher variability in the ***g*** and ***A*** parameters is encountered for the more flexible coordination geometry of **2** and **4**.

Magnetization dynamics. The magnetization dynamics of compounds **1**–**4** have been investigated by AC susceptometry on polycrystalline samples. The thermal variation of the magnetic susceptibility in a zero static magnetic field reveals no imaginary component of the susceptibility (χ'') in the whole investigated temperature range (10–80 K for **1** and **3**, and 5–40 K for **2** and **4**). When a small static magnetic field (> 40 mT) is applied, slow magnetic relaxation is observed with appearance of a peak in the imaginary component of the susceptibility and a concomitant decrease of the real part (χ') (Figures S5-S12).

Under a static magnetic field of 1.0 T, all compounds show slow relaxation of the entire magnetization, so that, this field was selected to investigate the temperature dependence of the relaxation time τ, which is representative of spin-lattice relaxation. The frequency dependences of χ'' are well reproduced with the Debye model (Figures S5-S8) and the extracted values of τ as a function of the temperature are reported in Figure 3.

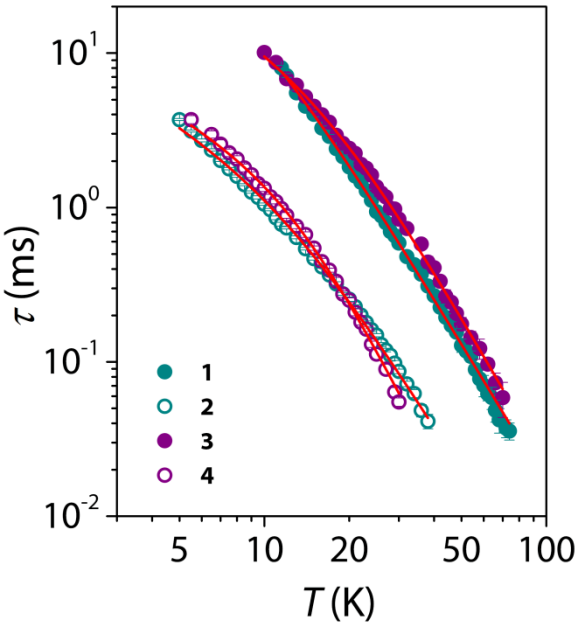

Figure 3. Temperature dependence of τ extracted from AC susceptibility measurements for microcrystalline powders of compounds **1**–**4** under an applied static magnetic field of 1.0 T. Solid lines are the best-fit of the model (see text).

The oxovanadium(IV) complexes **1** and **3** show slow magnetic relaxation up to ca. 70–80 K with exceptionally long relaxation times. They range from ca. 10 ms at 10 K to ca. 0.040–0.060 ms at 75 K. The vanadium(IV) complexes **2** and **4** also show slow relaxation of the magnetization, but with relaxation times which are a factor of ca. 10 lower with respect to the oxovanadium(IV) counterparts. More specifically, they range from ca. 4.0 ms at 5 K to ca. 0.050–0.072 ms at 30 K, above which they are not measurable.

The temperature dependence of τ, reported in Figure 3 in a $log(\tau)$ *vs* $log(T)$ plot, shows for all compounds a change in the slope of the curve as the temperature increases. This is almost unperceivable for **1** and more pronounced for **4**. This behaviour is indicative of the competition between the direct and the Raman mechanism of relaxation, the former dominating at lower temperature with respect to the latter. To account for these two contributions to the relaxation, the spin-lattice relaxation rate, τ^{-1}, was fitted (solid lines in Figure 3) with the following model

$$\tau^{-1} = aT + bT^n \qquad (1)$$

where a is the coefficient of the direct mechanism, while b and n are the coefficient and the exponent of the Raman mechanism, respectively.[17,18,20] This model satisfactorily reproduces the T dependence of τ with the best-fit parameter reported in Table 2.

Table 2. Best-fit parameters of the model used (eq. 1) to reproduce the temperature dependence of the spin-lattice relaxation rate for **1**–**4**.

Compound	a ($\mu s^{-1} K^{-1}$)	b ($\mu s^{-1} K^{-n}$)	n
1	4.0(5)	0.051(7)	3.0(1)
2	51(1)	0.38(1)	3.0(1)
3	7.8(4)	0.016(3)	3.2(1)
4	49(2)	0.049(2)	3.7(1)

The values of the Raman exponent n (ca. 3) are particularly low with respect to what is expected for paramagnetic centers in inorganic solids.[29] However, values of ca. 3 are commonly observed for vanadium(IV)-based molecular systems investigated through both AC susceptometry and pulsed EPR spectroscopy.[17,18,20]

Remarkably, the relaxation times observed for the oxovanadium(IV) derivatives **1** and **3** are the highest values obtained among the vanadyl-based molecular spin qubits studied up to date,[17,18,20,22] excluding the case in which τ is further increased at low temperatures as a

result of spin-phonon bottleneck effects due to the crystallites size.[30] Such long relaxation times allow to follow the dynamics of **1** and **3** up to ca. 80 K with a slow relaxation process that is detected even above this temperature (Figures S5 and S7). Moreover, the poor efficiency of the spin relaxation mechanisms herein involved allows to observe quite long relaxation times in a relatively wide temperature range also for the octahedral complexes **2** and **4** (Figure 3).

It is worth noting that both square pyramidal oxovanadium(IV) complexes **1** and **3** show very similar absolute values of the relaxation times and very similar temperature dependences independently from the structural modification introduced through the ligand. Analogous consideration hold for the octahedral complexes **2** and **4**. This confirms our previous observations on the role played by the different orbital contribution to the ground state in determining the enhancement of the absolute values of τ when passing from the square pyramidal to the octahedral coordination.[20] Interestingly, a factor of ca. 10 between the values of τ for square pyramidal *versus* octahedral complexes were also observed for the $[VO(dmit)_2]^{2-}$ / $[V(dmit)_3]^{2-}$ (dmit = 1,3-dithiole-2-thione-4,5-dithiolate) pair of complexes.[20]

In order to get better insights on the relaxation mechanisms involved in such compounds, the relaxation time was also investigated as a function of the static magnetic field in a wide field range (0.0–8.5 T) at different temperatures. The relaxation times extracted with the Debye model (Figures S9-S12) for **1**–**4** are reported in Figure 4.

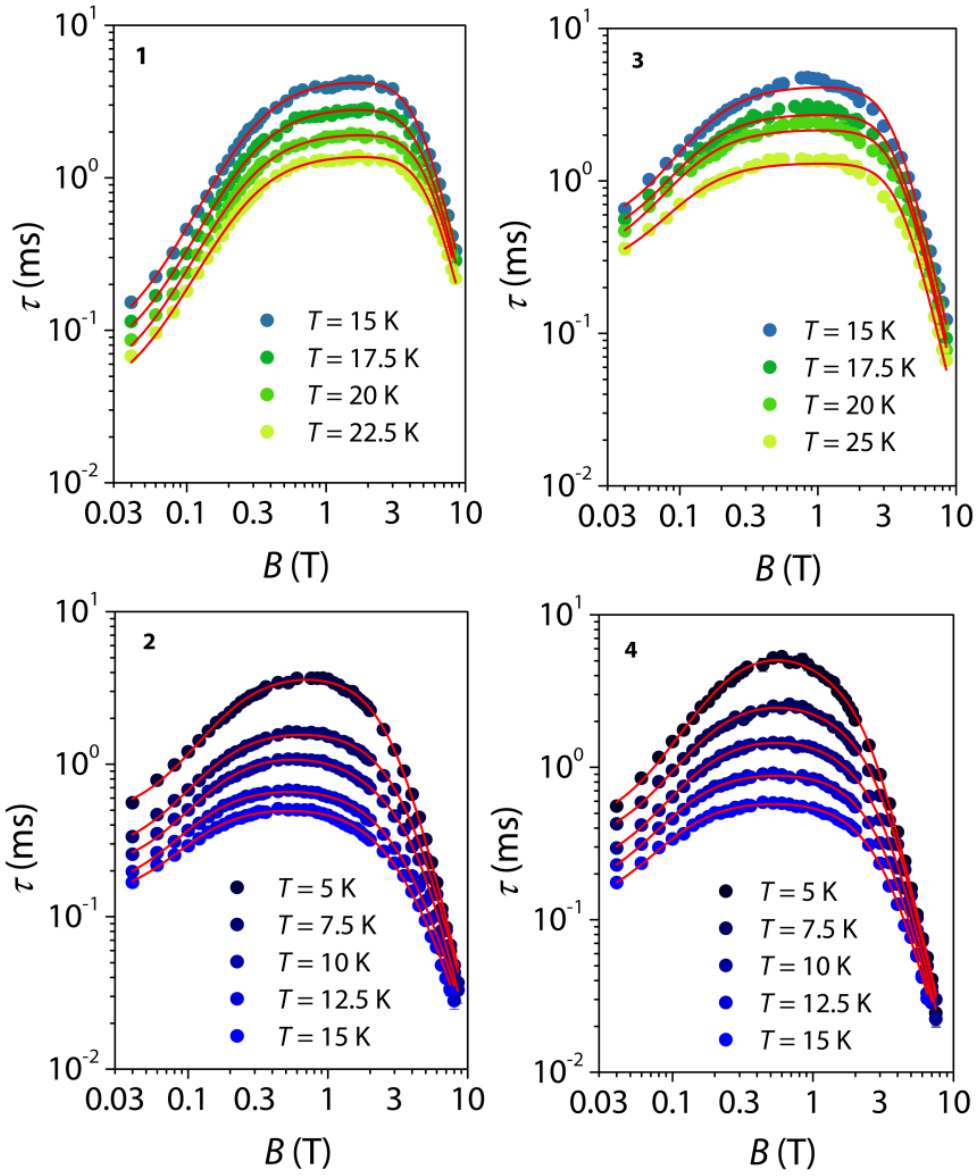

Figure 4. Magnetic field dependence of τ extracted from AC susceptibility measurements for compounds **1**–**4** at different temperatures (see legends). Solid lines are the best-fits of the models (see text).

The field dependences of the relaxation time for **1**–**4** show three main common features *i)* a rapid increase of τ up to ca. 0.4 T at low fields, *ii)* an almost unchanged relaxation time at intermediate fields, whose wideness varies as a function of the investigated compound, and *iii)* a rapid decrease of the relaxation time at high fields. This common non-monotonous behavior is similar to what already reported for closely related systems,[17,18,20,22] and reflects two antagonist effects of the magnetic field: *i)* a rapid relaxation promoted at low fields by spin-spin and spin-nuclei interactions, and *ii)* a more efficient spin-phonon direct mechanism of relaxation at high fields ($\tau \propto B^4$). The mixing of the energy levels due to spin-spin and spin-nuclei interactions is indeed suppressed by increasing the field strength, while

the more efficient direct mechanism of relaxation at high field is due to the higher phonon density that match the energy separation between the $m_S = \pm½$ levels. To account for these two contributions, the B dependence of the relaxation rate is usually reproduced with the Brons - van Vleck model[31,32]

$$\tau^{-1} = cB^4 + d\frac{1+eB^2}{1+fB^2} \qquad (2)$$

where the first term corresponds to the direct mechanism of relaxation, while the second term takes into account the effect of an internal magnetic field in promoting relaxation, considered as a sum of spin-nuclei hyperfine and spin-spin dipolar interactions.

The B dependence of τ for the oxovanadium(IV) compounds **1** and **3** herein investigated is well reproduced through the Brons - van Vleck model (Eq. 2), whereas the vanadium(IV) compounds **2** and **4** requires the extended Brons - van Vleck model (Eq. 3) recently developed,[22] to provide an adequate fit of the experimental data (Figure S13).

$$\tau^{-1} = cB^4 + d\frac{1+eB^2}{1+fB^2} + g\frac{1+eB^2}{1+hB^2} \qquad (3)$$

The best-fit parameters are reported in Table S2.

The results of the fit indicate that both oxovanadium(IV) complexes **1** and **3** show a field dependence of the relaxation time that is appropriately described as sum of a direct mechanism of relaxation at high fields (above ca. 4 T and 3 T for **1** and **3**, respectively) plus a contribution of the internal field type at low fields. On the contrary, the field dependence of the relaxation time for both vanadium(IV) complexes **2** and **4** is appropriately described as sum of a direct mechanism of relaxation at high fields (above ca. 1 T and 0.7 T for **2** and **4**, respectively) plus two contributions of the internal field type at low fields.

We have recently found that the d parameters, extracted from the fit of the magnetic field dependence, follows an exponential temperature dependence.[22] The resulting Arrhenius behavior allowed us to extract effective energy values, U_{eff}, which also well correlate with the experimental low energy vibrational modes detected by time-domain THz spectroscopy. Interestingly, a complex behaviour of the magnetic field dependence of τ has been found to be accompanied by the presence of more than one predominant low energy vibration, which shows a correlation between the energy levels and the frequency of the involved phonon of the type $U_{eff} = h\omega_\alpha/2$. The same relation has been theoretically proposed for the relaxation

time of SMM characterized by excited magnetic states at high energy, when the anharmonicity, or finite linewidth, of vibrational modes is taken into account.[24]

In this case, the analysis of the *T* dependence of the *d* parameter extracted by the field dependence measurements performed at various temperatures provides a unique value of U_{eff} for **1** (U_{eff} = 24(2) cm^{-1}) and for **3** (U_{eff} = 17(2) cm^{-1}) (Figure S14). Indeed, the linear fit of *ln(d)* and *ln(g)* versus T^{-1} provides U_{eff} = 6(1) cm^{-1} and 10(1) cm^{-1} for **2**, and U_{eff} = 9(1) cm^{-1} and 16(1) cm^{-1} for **4**, respectively (Figure S14). In general, the magnetic analysis suggests that the tris-chelated vanadium(IV) complexes have lower energy vibrational modes which act as efficient mediators of spin-lattice relaxation with respect to the oxovanadium(IV) derivatives.

The record spin-lattice relaxation times observed for **1** are in agreement with the predicted higher activation energy involved in the relaxation (ca. 48(4) cm^{-1}) with respect to the one (40 cm^{-1}) of the best performing system identified to date, namely [VO(acac)$_2$] (acac = acetylacetonate), which shows slightly lower values of τ (Figure S15).[30] This suggests that the lowest energy vibrational modes are expected to be higher in energy for **1** with respect to [VO(acac)$_2$] Moreover, the presence of more than one vibrational mode involved in the relaxation for the octahedral complexes seems again responsible for specific modifications of the overall values of τ as a function of the magnetic field *B*, in this case reducing the wideness of the plateaux at intermediate fields where τ is maximum. Indeed, passing from **1** to **3** the width of the plateaux is slightly reduced, while it is strongly reduced passing to **2** and **4**, both showing very similar behaviours.

FT-IR and THz Vibrational Spectroscopy. An accurate determination of the energy of the vibrational modes active in these compounds is crucial for a better understanding of the correlation between vibrational modes and the spin dynamics. We have thus collected room-temperature infrared (4000–400 cm^{-1}) and THz (100–20 cm^{-1}) spectra, the latter through time-domain THz spectroscopy, of the protonated ligands H$_2$cat and H$_2$naph-cat. The comparison between the spectra indicates that the structural modification herein introduced by expanding the structure of the ligand from one to two condensed aromatic rings has important implications on the overall molecular rigidity. Indeed, in the middle-infrared region most of the absorption peaks related to the aromatic skeleton vibrations of H$_2$naph-cat are shifted toward higher energies when compared to H$_2$cat (Figure S16).[33] The low energy vibrations detected by room-temperature time-domain THz spectroscopy are also affected by the

skeleton rigidity. Indeed, the predominant lowest energy absorption occurs at a frequency ca. 10 cm^{-1} higher for the H_2naph-cat ligand with respect to the H_2cat one (Figure 5).

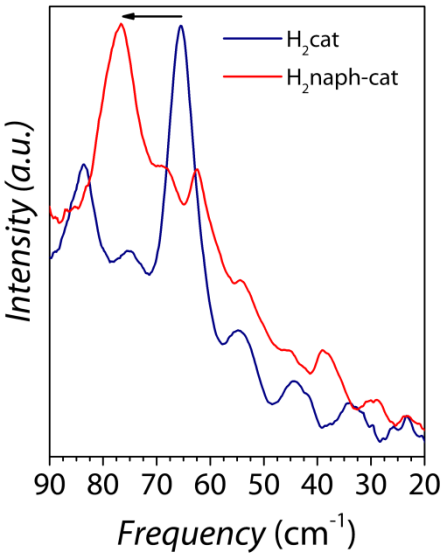

Figure 5. Comparison between experimental THz (20–90 cm^{-1}) spectra of H_2cat and H_2naph-cat ligands. Arrows indicate the shift towards higher frequencies of the lowest energy vibrational mode.

These findings are in agreement with what was previously reported for the 1,4-dihydroxy isomers of the 1,2-dihydroxy compounds herein investigated.[34,35]

When passing to the vibrational spectra of the complexes, the middle-infrared regions of **1** and **2** do not show substantial differences between the two compounds, except for the presence of an extra absorption peak at ca. 942 cm^{-1} for **1**, which is clearly relatable to the V=O stretching normal mode (Figure S17). These results are not surprising due to the strictly local nature of the molecular vibrational modes falling in this spectral region, and are in agreement with previous findings.[20] Analogous results are observed comparing the spectra of **3** and **4**. Indeed, they show very similar spectra except for the extra peak at ca. 958 cm^{-1} (V=O stretching) for **3** (Figure S18).

The comparison between the middle-infrared spectra of **1** and **3** provides instead some insights on the role of the structural rigidity introduced through the ligand. Excluding the vibrational modes related to the PPh_4^+ counterion falling at ca. 1105, 995, 754, 722, 687, 623, and 528 cm^{-1}, the higher rigidity of the two condensed rings in the naph-cat^{2-} ligand with respect to the cat^{2-} allows a slight shift towards higher frequency of some specific vibrational modes centered at ca. 1255, 948, and 535 cm^{-1} (Figure 6a), including the V=O stretching vibrational mode. The same considerations are valid for the octahedral complexes **2** and **4** (Figure 6b).

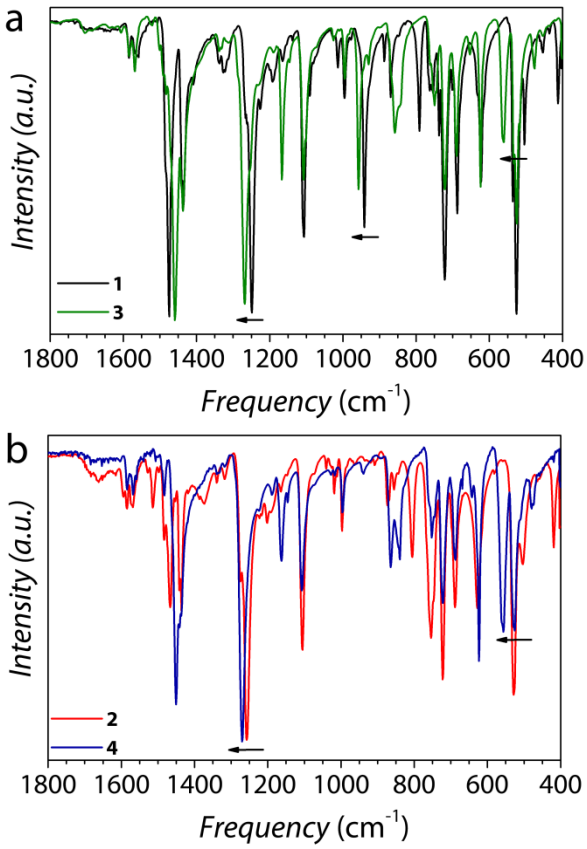

Figure 6. Comparison between infra-red spectra (1800–400 cm^{-1}) of compounds **1** and **3** (a) and **2** and **4** (b). Arrows indicate the shift towards higher frequencies of naph-cat complexes both in square pyramidal (a) and octahedral (b) coordination geometries. The additional signal observed in the spectra of **1** and **3** is ascribed to the V=O bond stretching.

Room-temperature time-domain THz spectra were recorded in the 0.3–3.0 THz range (10–100 cm^{-1}) to characterize the low energy vibration frequencies of compounds **1**–**4** (Figure 7).

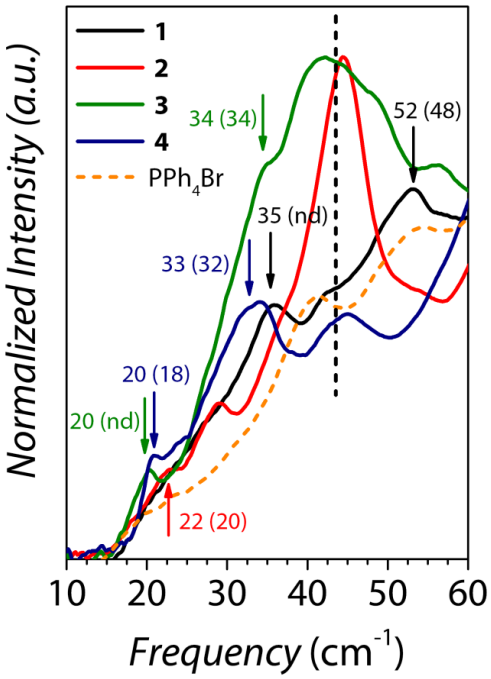

Figure 7. Vibrational spectra in the 0.3–1.8 THz range (10–60 cm^{-1}) of compounds **1**–**4** and $(Ph)_4PBr$ for comparison (orange dashed line). Arrows indicates the lowest energy absorptions for all compounds together with experimental frequencies and those found through magnetic susceptibility analysis (in parenthesis). nd = not determined through magnetic analysis.

In general, the THz spectra of compounds **1**–**4** appear more complicated with respect to those of $[VO(acac)_2]$ and $[VO(Et_2dtc)_2]$ already studied.[22] This might be partially related to the presence of the PPh_4^+ counterion, that was absent in the previously studied compounds, as well as to the possible mixed nature of low energy intermolecular vibrations with rotational components, as recently highlighted through a density functional theory study performed on a model compound.[25]

The spectra of the oxovanadium(IV) complexes **1** and **3** show lowest energy absorptions at ca. 35 and 52 cm^{-1} for **1**, and 20 and 34 cm^{-1} for **3**, respectively. Interestingly, in this frequency region the lowest energy vibrational modes are shifted toward higher frequencies for the complex of the smaller cat^{2-} ligand with respect to that of the naph-cat^{2-}, which is in agreement with the magnetic analysis. More specifically, considering the previously observed relation ($U_{eff} = h\omega_\alpha/2$),[22,24] the magnetic analysis suggests that the phonon involved in the relaxation mechanism should have a frequency of 48 cm^{-1} and 34 cm^{-1}, for **1** and **3**, respectively, which agree with the spectroscopic findings. Both **1** and **3** show one additional peak at lower frequencies that was not determined through the magnetic analysis. According to a recently reported study on the role of intramolecular vibrations as mediators of

spin-lattice relaxation, each vibrational mode should couple with the spin in a different extent as a function of the type of vibration and electron occupancy in the metal *d*-orbitals.[23] More specifically, it has been observed that for the compound $[(Ph)_4P]_2[Cu(mnt)_2]$ (mnt = 1,2-dicyanoethilene-1,2-dithiolate), which has been theoretically investigated, only 3 out of 16 calculated vibrational modes in the 0–150 cm^{-1} range were identified as effective in mediating spin-lattice relaxation, with the first active low energy mode which is the fourth in energy (at ca. 35 cm^{-1}). Consequently, it might be not surprising if the lowest energy vibrational mode observed herein for **1** and **3** is not strongly coupled with the spin to promote efficient relaxation, and consequently does not contribute substantially to the fine-structure of the τ versus B behaviour (*vide infra*). This hypothesis is corroborated by the fact that both **1** and **3**, which share the same coordination geometry, show the same feature. Accordingly, the nature of the lowest energy detected vibrational mode for **1** and **3** is likely to be the same, with a different resonating frequency due to the different ligand mass.

The spectra of the vanadium(IV) complexes show, in general, low energy absorption bands which are shifted toward lower energies with respect to the oxovanadium(IV) complexes, again in agreement with the findings of the magnetic analysis. More specifically, **2** and **4** show lowest energy absorptions at 22 cm^{-1} and ca. 28 cm^{-1} for **2**, and 20 cm^{-1} and 33 cm^{-1} for **4**. All these values agree with what found through the magnetic analysis, *i.e.* two resonating phonons for **4** at 18 cm^{-1} and 32 cm^{-1}, and two for **2** at 20 cm^{-1} and 12 cm^{-1}, the lowest in energy not detectable due to the low signal available below 15 cm^{-1}.

Finally, it should be remarked that all spectra show one common absorption peak at ca. 43 cm^{-1} (vertical dashed black line in Figure 7), apparently not involved in the relaxation, which well agrees to the first observable vibrational mode of the PPh_4^+ counterion (dotted orange line in Figure 7).

Pulsed Electron Paramagnetic Resonance Spectroscopy. Coherence times (T_m) and spin-lattice relaxation times (T_1) for compound **1** were measured at X-band in the 4.5–100 K temperature range. The measurements were performed at the so-called “powder-line” of the echo-detected field-swept (EDFS) EPR spectrum (see arrow in Figure 8a). The spectral features of the EDFS EPR spectrum reflect those of the corresponding CW-EPR spectrum (Figure 2a) although some distortions are present at the high field end of the spectral pattern due to field-dependent nuclear modulation effects and orientation-dependent relaxation times.

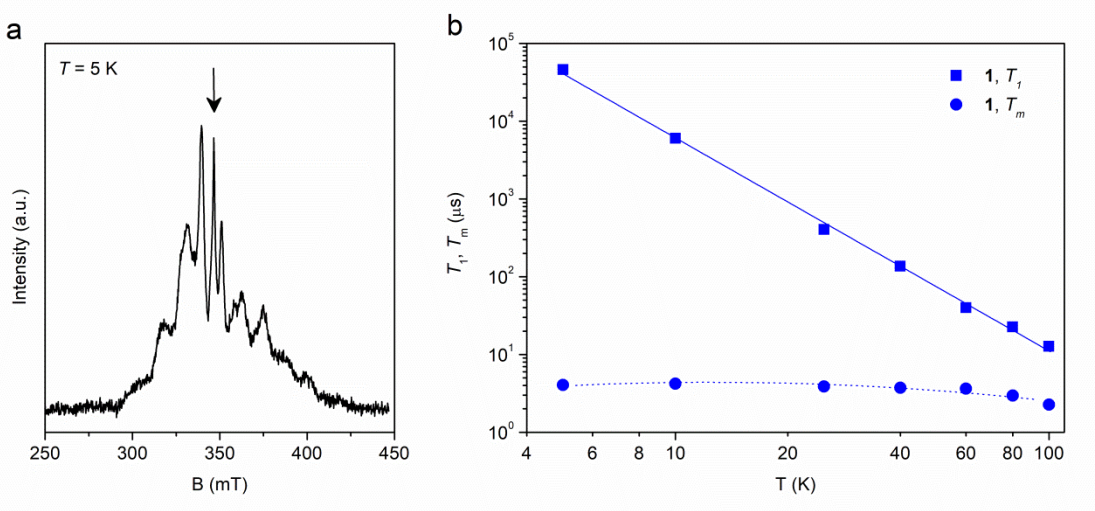

Figure 8. Experimental X-band (9.7 GHz) ED-EPR spectrum of **1** (1.0 mM in CH_2Cl_2:C_6H_6 3:1) recorded at 5 K (a). The arrow indicates the magnetic field setting at which pulse EPR experiments were performed; Temperature dependence of T_1 and T_m for **1** (b). The solid line is the best-fit of the model (see text). The short-dashed line represents a guide for the eyes. Error bars are within the size of the symbols.

The thermal variation of T_1 for **1** was obtained by inversion recovery experiments performed in the 4.5–100 K temperature range. The resulting saturation recovery traces were fitted with a stretched monoexponential equation

$$I = I_0 + k_1 exp\left[-\left(\frac{\tau_p}{T_1}\right)^{\beta_1}\right] \qquad (4)$$

and the extracted T_1 values are reported in Figure 8b (squares). The thermal variation of T_1 for **1** shows a constant slow decrease from the maximum values of ca. 42 ms at 4.5 K, to the lowest, but still remarkable value of 12.67 μs at 100 K. This indicates that measurable values of T_1 were available at higher temperatures if the temperature range were not limited by the melting point of the frozen solution. As shown in Figure 8b, T_1 exhibits a linear temperature dependence behavior, which has been modeled assuming only one predominant contribution of Raman type to the relaxation with n = 2.8(2), in agreement with the AC susceptibility data (*vide supra*).

To investigate the quantum coherence in details and to quantify the phase memory time, T_m, of **1** as a function of the temperature, echo decay experiments were also performed.

The decay traces were fitted using the stretched-exponential equation

$$I = I_0 + k_m exp\left[-\left(\frac{2\tau_p}{T_m}\right)^{\beta m}\right] \qquad (6)$$

as usually done for transition metal-based systems,[36] where I indicates the echo intensity, $2\tau_p$ is the delay between the initial pulse and the echo detection and β_m is the stretch factor.

The thermal variation of T_m for **1** shows an almost temperature independent behavior in the 4.5–60 K range, with values of T_m within 4.2–3.6 μs. Then, T_m slightly decreases to 3.0 μs at 80 K and 2.3 μs at 100 K, most likely as a result of the significant decrease of T_1 in that temperature range (Figure 8b).

It should be highlighted that the values of T_m observed at low temperature of ca. 4.0 μs are, in general, higher than those already reported so far in the literature for similar compounds measured in analogous protiated solvent matrixes.[37] Moreover, they are slightly higher than those reported for vanadyl complexes containing nuclear spin-free ligands (ca. 3.0-3.5 μs), which are characterized by a more abrupt decrease of T_m as the temperature increases.[37]

CONCLUSIONS

In conclusion, we investigated the spin-lattice relaxation of four V^{IV} based potential molecular qubits where specific structural modifications have been introduced to find clear correlations between the spin dynamics and the role played by low energy vibrational modes as mediators of spin-lattice relaxation. Both the influence of the different coordination geometries, *square-pyramidal* versus *octahedral*, as well as the increased rigidity of the coordinating ligand have been correlated to the observed spin-lattice relaxation.

The analysis of the temperature dependence of the relaxation time did not show any significant differences between catecholate and naphthalene-catecholate complexes, whilst substantial differences between square pyramidal and octahedral complexes were observed. Indeed, the former provide longer relaxation times of a factor of ca. 10 with respect to the latter. This result allowed us to observe record relaxation times up to 80 K for **1** and **3**, and, more importantly, to define new specific design criteria for the preparation of highly coherent molecular spin qubits. A factor of ca. 10 was indeed also observed for another independent pair of vanadium and oxovanadium(IV) complexes with a different ligand, thus indicating that the specific coordination geometry plays a crucial role on the absolute values of the relaxation time not simply by generically increasing them, but enhancing the relaxation times by a specific factor, independently form the coordinating ligand structure.

From this comparative study further insights emerge on the role played by the coordinating ligand. Since no substantial changes have been evidenced as a function of the

mass and the rigidity of the ligand, the nature of the bonding between the metal center and the donor atoms seems fundamental in determining the magnitude of the relaxation times once the coordination geometry is kept fix. This may be due either to the fine-modulation of the electronic parameters of the metal centers, or to the specific force of the vibrational modes related to the *metal-donor atoms* bonds. Indeed, the relaxation times herein observed are higher than those observed for vanadyl β-diketonate derivatives recently studied, and those observed for complexes where the ligands have sulphur donor atoms, such as the 1,3-dithiole-2-thione-4,5-dithiolate ($dmit^{2-}$) and diethyldithiocarbamate (Et_2dtc^-) ligands (Figure S15), which have longer V–S bond distances.

While the analysis of the temperature dependence of the relaxation time is well described for all complexes by the sum of the direct and the Raman relaxation mechanisms, and appears independent from the molecular structure of the ligand, important differences are observed when the field dependence of τ is concerned. The analysis of the field dependent data confirms the generality of the Arrhenius-type dependence related to the efficiency of the processes responsible for the non-monotonic field dependence of the relaxation time. This allowed to find further correspondence between the activation energy values obtained by this magnetic analysis and the frequency of the low energy phonons spectroscopically detected by time-domain THz spectroscopy. Unfortunately, clear correlations with the nature of vibrational modes involved cannot be performed with certitude as a consequence of the spectra complexity, which is further enhanced by the presence of the counterion.

It also emerges from this study that the naphthalene-catecholate, identified by experimental middle-infrared and THz spectra as a ligand more rigid than the catecholate one, does not provide substantial enhancement of the relaxation times, nor allow to maximize the plateaux where τ is maximum as a function of the magnetic field strength. This is related to the fact that *i)* the molecular structure of the ligand seems not crucial in determining the absolute values of the relaxation time, which seems predominantly determined by the coordination geometry and the nature of the donor atoms, as already indicated above, and *ii)* the analysis of the lowest energy vibrational modes by time-domain THz spectroscopy has revealed that compound **3** has the first low energy vibrational modes at slightly lower energy with respect to that of **1**, independently from the shift towards higher frequencies observed at higher frequency regions. This latter point might be due to the mixing between low energy vibrational modes with rotational components, the latter expected to be at higher energies for smaller masses.

Thanks to disentanglement of the two main contributions to the overall molecular rigidity of potential molecular qubits, *i.e.* the metal coordination environment and the molecular structure of the ligand, we can conclude that the previous points emerge as fundamental insights for the design of highly coherent molecular systems.

Finally, we have demonstrated that this multitechnique approach based on AC susceptometry combined with THz spectroscopy is a powerful tool for the identification of highly coherent molecular spin qubits. Indeed, the most performing system identified herein, compound **1**, shows long quantum coherence times of ca. 4.0 μs in the 4.5–60 K range, that well compare with the most performing results obtained so far for molecular spin qubits.

EXPERIMENTAL SECTION

Synthesis.

$[(Ph)_4P]_2[VO(cat)_2]$ (1). An aqueous solution (15 mL) of $VOSO_4 \cdot xH_2O$ (1.0 g, 6.0 mmol) was refluxed overnight with NaOH (0.32 g, 8.0 mmol) resulting in the formation of a green precipitate. The solid was filtered, washed with cold water, and added in portions to an aqueous solution (15 mL) of catechol (1.1 g, 10.0 mmol) and an excess of NaOH (1.2 g, 30.0 mol). A methanol solution (5 mL) of tetraphenylphosphonium bromide (5.0 g, 12.0 mmol) was added dropwise to the resulting green solution with precipitation of **1** as a green-grey microcrystalline solid. The precipitate was separated from the mother liquor by vacuum filtration, washed several times with water, and dried under vacuum. Yield 85%. Compound **1** was recrystallized by addition of acetone to a CH_2Cl_2 solution, which gives green shiny crystals suitable for X-ray analysis. Elemental anal. calcd for $C_{60}H_{48}O_5P_2V$: C, 74.92; H, 5.03; found: C, 73.91; H, 5.05. FT-IR ($\bar{\upsilon}_{max}/cm^{-1}$, KBr pellet): 3049w, 2995w, 1584w, 1560vw, 1474vs, 1435s, 1409w, 1340w, 1322w, 1249vs, 1193w, 1163w, 1106s, 1013w, 995m, 942m (ν V=O), 887w, 870m, 791m, 762m, 753m, 738m, 723s, 688s, 623s, 526vs, 504m, 453w, 412m.

$[(Ph)_4P]_2[V(cat)_3]$ (2). An aqueous solution (10 mL) of $VOSO_4 \cdot xH_2O$ (0.550 g, 2.7 mmol) was added dropwise to an aqueous solution (20 mL) of catechol (0.890 g, 8.1 mmol) and NaOH (0.400 g, 10.0 mmol). A methanol solution (5 mL) of tetraphenylphosphonium bromide (2.85 g, 6.8 mmol) was added dropwise to the resulting blue solution with precipitation of **2** as a blue microcrystalline solid. The precipitate was separated from the mother liquor by vacuum filtration, washed several times with water, and dried under

vacuum. Yield 78%. Compound **2** was recrystallized by slow diffusion of Et_2O vapours to a MeOH solution, which gives deep-blue block crystals suitable for X-ray analysis. Elemental anal. calcd for $C_{66}H_{52}O_6P_2V$: C, 75.21; H, 4.97; found: C, 75.62; H, 4.95. FT-IR ($\bar{\upsilon}_{max}/cm^{-1}$, KBr pellet): 3049w, 2995w, 1585w, 1569vw, 1513m, 1483m, 1467vs, 1435s, 1372w, 1340w, 1317w, 1258vs, 1201w, 1163w, 1106s, 1013w, 995m, 870m, 855w, 805m, 754m, 738m, 723s, 688s, 623s, 526vs, 504m, 463w, 420m.

$[(Ph)_4P]_2[VO(naph\text{-}cat)_2]$ (3). An aqueous solution (10 mL) of $VOSO_4 \cdot xH_2O$ (0.330 g, 2.0 mmol) was added dropwise to an aqueous solution (20 mL) of catechol (0.60 g, 3.75 mmol) and NaOH (0.450 g, 11.2 mmol). A methanol solution (5 mL) of tetraphenylphoshonium bromide (2.0 g, 4.70 mmol) was added dropwise to the resulting green solution with precipitation of **3** as a green microcrystalline solid. The precipitate was separated from the mother liquor by vacuum filtration, washed several times with water, and dried under vacuum. Yield 87%. Compound **3** was recrystallized by addition of acetone to a freshly prepared CH_2Cl_2 solution, which gives green shiny microcrystals. Elemental anal. calcd for $C_{68}H_{52}O_5P_2V$: C, 76.90; H, 4.94; found: C, 76.15; H, 4.73. FT-IR ($\bar{\upsilon}_{max}/cm^{-1}$, KBr pellet): 3053w, 3004w, 1584w, 1567vw, 1459vs, 1437s, 1340w, 1322w, 1269vs, 1190w, 1167m, 1107m, 995w, 958m (ν V=O), 857m, 749m, 738m, 723s, 688s, 652w, 624m, 560m, 525s, 476w, 453w.

$[(Ph)_4P]_2[V(naph\text{-}cat)_3]$ (4). Compound **4** was obtained by slow conversion of **3** in CH_2Cl_2 solution. Slow evaporation of the solvent provides deep-blue block crystals suitable for X-ray analysis. Elemental anal. calcd for $C_{78}H_{58}O_6P_2V$: C, 77.80; H, 4.85; found: C, 77.67; H, 4.81. FT-IR ($\bar{\upsilon}_{max}/cm^{-1}$, KBr pellet): 3044w, 3000w, 1584w, 1567vw, 1482w, 1450vs, 1440s, 1436s, 1340w, 1322w, 1269vs, 1190w, 1167m, 1107m, 995w, 864m, 839m, 749m, 738m, 723s, 688s, 642w, 624m, 560m, 525s, 476w, 453w.

Characterization. C, H, N analyses were performed with a *CHN-S Flash E1112 Thermofinnigan* analyzer. FT-IR spectra were performed on KBr pellets and collected with a *Shimadzu-8400S* spectrophotometer.

Single Crystal X-Ray Crystallography. Single crystal X-ray diffraction measurements were performed on an *Oxford Xcalibur PX Ultra - Onyx CCD* diffractometer, using an Enhance Ultra X-ray graphite-monochromated Cu*Kα* (λ = 1.540 Å) or Mo*Kα* (λ = 0.7107 Å) radiation.

The structures were solved by direct methods (SHELXS-97) and refined on F^2 with full-matrix least squares (SHELXL-97),[38] using the Wingx software package.[39] All non-H atoms were refined with anisotropic displacement parameters. Graphical material was prepared using Mercury CSD 3.9.[40] A summary of the crystallographic data and the structure refinement for compounds **1**, **2** and **4** is reported in Table 3.

Table 3. Summary of X-ray crystallographic data for **1**, **2**, and **4**.

	1	**2**	**4**
Empirical formula	$C_{60}H_{48}O_5P_2V$	$C_{66}H_{52}O_6P_2V$	$C_{78}H_{58}O_6P_2V$
Formula weight	961.86	1053.96	1204.12
Crystal size, mm	0.50 × 0.30 × 0.30	0.30 × 0.20 × 0.15	0.20 × 0.20 × 0.10
Crystal system	Monoclinic	Monoclinic	Monoclinic
Space group	*P2₁/c*	*C2/c*	*P2₁/n*
a, Å	13.2529(2)	15.3120(8)	11.1798(5)
b, Å	12.2534(1)	13.2289(7)	27.8301(14)
c, Å	29.1923(3)	25.317(1)	19.4916(13)
α, deg.	90	90	90
β, deg.	92.804(1)	102.016(6)	103.704(5)
γ, deg.	90	90	90
V, Å^3	4734.95(9)	5015.9(5)	5891.9(6)
Z	4	4	4
T, K	100(2)	100(2)	100(2)
ρ (calc), Mg/m^3	1.349	1.396	1.357
μ, mm^{-1}	2.805	0.319	2.385
θ range, deg.	4.40–72.40	4.11–26.32	4.19–68.00
GooF	1.034	1.038	0.933
*R*1	0.0567	0.0633	0.0882
*wR*2	0.1384	0.1473	0.1528

$R1 = \Sigma||F_o|-|F_c||/\Sigma|F_o|$, $wR2 = [\Sigma[w(F_o^2-F_c^2)^2]/\Sigma[w(F_o^2)^2]]^{1/2}$, $w = 1/[\sigma^2(F_o^2) + (aP)^2 + bP]$, where $P = [\max(F_o^2,0) + 2F_c^2]/3$.

Full crystallographic data for the solved structures have been deposited in the Cambridge Crystallographic Data Centre with CCDC numbers 1572974 (**1**), 1572976 (**2**), 1572975 (**4**), respectively.

Electron Paramagnetic Resonance. CW X-Band EPR spectra of all samples were recorded on a *Bruker Elexsys E500* spectrometer equipped with a SHQ cavity (ν = 9.30 GHz). Low temperature measurements were obtained using an *Oxford Instruments ESR900* continuous flow helium cryostat. Pulsed EPR measurements were carried out with a *Bruker Elexsys E580*

at X-band ($\nu \cong 9.70$ GHz) equipped with a flexline dielectric ring ENDOR resonator (*Bruker EN 4118X-MD4*). Temperatures between 4.5 and 100 K were obtained with *an Oxford Instruments CF935* continuous flow helium cryostat. Echo detected field swept EPR spectra were recorded by using the Hahn Echo pulse sequence ($\pi/2$—τ — π —τ —*echo*) with fixed interpulse delay time τ = 200 ns, $t_{\pi/2}$ = 16 ns and t_{π} = 32 ns. Phase memory times were measured both by the Hahn Echo sequence upon increasing the interpulse delay τ starting from τ = 98 ns. Spin-lattice relaxation times were measured using the standard inversion recovery sequence (π—t_d—$\pi/2$—τ—π —τ—*echo*), with $\pi/2$ = 16 ns. The uncertainty in T_1 estimated from replicate measurements was 5%–10% depending upon the signal-to-noise ratio at a given temperature-field combination.

Magnetic measurements. AC susceptibility measurements were performed in the temperature range 5.0–80 K with applied magnetic fields up to 8.5 T on polycrystalline samples of compounds **1** (56.12 mg), **2** (48.10 mg), **3** (54.20 mg), and **4** (45.00 mg) by using a *Quantum Design Physical Property Measurement System (PPMS)* equipped with a AC susceptometer operating in the 10 Hz–10 kHz frequency range. Susceptibility data were corrected for the sample holder previously measured using the same conditions and for the diamagnetic contributions as deduced by using Pascal's constant tables.[41]

THz time-domain spectroscopy set-up. THz spectra were measured by time-domain spectroscopy using a table-top experimental set-up and acquisition procedure that enables to achieve a very high signal to noise, higher than what is commonly achieved in the standard far-infrared investigations. Moreover, the accurate analysis of the data enables to disentangle the signals from spurious contributions coming from the multiple reflections. The detailed description of the experimental set-up and the data analysis procedure is reported elsewhere.[42] We implemented a home-made THz-TDS system in transmission configuration, based on optical laser pulses (T-light 780 nm fiber laser, MenloSystems) and low-temperature GaAs photoconductive antennas. The emitted THz field is collimated and focused on the sample by a couple of parabolic off-axis mirrors. The signal transmitted through the sample is again collimated and focused on the detector, a second photoconductive antenna, biased by a second optical pulse; the antenna photocurrent is measured by a lock-in amplifier and an acquisition board. The electric field amplitude of the THz radiation is measured changing the time delay between the pump and probe pulses, so to reconstruct its temporal evolution. A home-made software acquires the processed signal together with the reading of the delay line encoder and

retraces the final time dependent THz field. The working chamber, containing the whole THz set-up, was purged with nitrogen to eliminate the numerous contributions of water vapour, present at the THz frequencies spanned by the experiment. In order to improve the data quality and reduce the effects of external perturbations during the acquisition (e.g. temperature fluctuations) measurements with and without sample are cyclically repeated.

We implemented a new method of data analysis,[42] which enables the extraction of the real physical material parameters (i.e. index of refraction, absorption coefficient and layer thickness). This method is based on an iterative fitting process of the transmission parameters and it takes into account the multiple reflection phenomena. The method applies to either the free standing single slab or multilayer system.

The spectra reported are measured in pellet samples of 13.2 mm diameter and thickness of about 0.7 mm. These are made by pressing under a manual hydraulic press (~ 0.8 GPa) a mixture of microcrystals and polyethylene powder (Merck).

ASSOCIATED CONTENT

Supporting Information

The Supporting Information is available free of charge on the ACS Publications website at DOI: XXXXX. Additional Figures and Data as mentioned in the text.

AUTHOR INFORMATION

Corresponding Authors

*E-mail:

*E-mail:

Notes

The authors declare no competing financial interest.

ACKNOWLEDGMENTS

European Research Council (ERC) through AdG MolNanoMaS (267746), Italian MIUR through the project Futuro in Ricerca 2012 (RBFR12RPD1) and the project PRIN 2015 (HYFSRT), and Fondazione Ente Cassa di Risparmio di Firenze are acknowledged for financial support.

REFERENCES

(1) Nielsen, M. A.; Chuang, I. L. *Quantum Computation and Quantum Information; Cambridge University Press: Cambridge,* **2000**.
(2) DiVincenzo, D. P. *Science* **1995**, *270*, 255.
(3) Knill, E.; Laflamme, R.; Milburn, G. J. *Nature* **2001**, *409*, 46.
(4) Blatt, R.; Wineland, D. *Nature* **2008**, *453*, 1008.
(5) Clarke, J.; Wilhelm, F. K. *Nature* **2008**, *453*, 1031.
(6) Pla, J. J.; Tan, K. Y.; Dehollain, J. P.; Lim, W. H.; Morton, J. J. L.; Jamieson, D. N.; Dzurak, A. S.; Morello, A. *Nature* **2012**, *489*, 541.
(7) Warner, M.; Din, S.; Tupitsyn, I. S.; Morley, G. W.; Stoneham, A. M.; Gardener, J. A.; Wu, Z.; Fisher, A. J.; Heutz, S.; Kay, C. W. M.; Aeppli, G. *Nature* **2013**, *503*, 504.
(8) Ardavan, A.; Rival, O.; Morton, J. J. L.; Blundell, S. J.; Tyryshkin, A. M.; Timco, G. A.; Winpenny, R. E. P. *Phys. Rev. Lett.* **2007**, *98*, 057201.
(9) Laucht, A.; Muhonen, J. T.; Mohiyaddin, F. A.; Kalra, R.; Dehollain, J. P.; Freer, S.; Hudson, F. E.; Veldhorst, M.; Rahman, R.; Klimeck, G.; Itoh, K. M.; Jamieson, D. N.; McCallum, J. C.; Dzurak, A. S.; Morello, A. *Sci. Adv.* **2015**, *1*, e1500022.
(10) Kennedy, T. A.; Colton, J. S.; Butler, J. E.; Linares, R. C.; Doering, P. J. *Appl. Phys. Lett.* **2003**, *83*, 4190.
(11) Balasubramanian, G.; Neumann, P.; Twitchen, D.; Markham, M.; Kolesov, R.; Mizuochi, N.; Isoya, J.; Achard, J.; Beck, J.; Tissler, J.; Jacques, V.; Hemmer, P. R.; Jelezko, F.; Wrachtrup, J. *Nat. Mater.* **2009**, *8*, 383.
(12) Tyryshkin, A. M.; Tojo, S.; Morton, J. J. L.; Riemann, H.; Abrosimov, N. V.; Becker, P.; Pohl, H.-J.; Schenkel, T.; Thewalt, M. L. W.; Itoh, K. M.; Lyon, S. A. *Nat. Mater.* **2012**, *11*, 143.
(13) Troiani, F.; Affronte, M. *Chem. Soc. Rev.* **2011**, *40*, 3119.
(14) Aromi, G.; Aguila, D.; Gamez, P.; Luis, F.; Roubeau, O. *Chem. Soc. Rev.* **2012**, *41*, 537.
(15) Bader, K.; Dengler, D.; Lenz, S.; Endeward, B.; Jiang, S.-D.; Neugebauer, P.; van Slageren, J. *Nat. Commun.* **2014**, *5*, 5304.
(16) Zadrozny, J. M.; Niklas, J.; Poluektov, O. G.; Freedman, D. E. *J. Am. Chem. Soc.* **2014**, *136*, 15841.
(17) Tesi, L.; Lucaccini, E.; Cimatti, I.; Perfetti, M.; Mannini, M.; Atzori, M.; Morra, E.; Chiesa, M.; Caneschi, A.; Sorace, L.; Sessoli, R. *Chem. Sci.* **2015**, *7*, 2074.
(18) Atzori, M.; Tesi, L.; Morra, E.; Chiesa, M.; Sorace, L.; Sessoli, R. *J. Am. Chem. Soc.* **2016**, *138*, 2154.
(19) Zadrozny, J. M.; Niklas, J.; Poluektov, O. G.; Freedman, D. E. *ACS Cent. Sci.* **2015**, *1*, 488.
(20) Atzori, M.; Morra, E.; Tesi, L.; Albino, A.; Chiesa, M.; Sorace, L.; Sessoli, R. *J. Am. Chem. Soc.* **2016**, *138*, 11234.
(21) Gatteschi, D.; Sessoli, R.; Villain, J. *Molecular Nanomagnets*; Oxford University Press: Oxford, UK, 2006.
(22) Atzori, M.; Tesi, L.; Benci, S.; Lunghi, A.; Righini, R.; Taschin, A.; Torre, R.; Sorace, L.; Sessoli, R. *J. Am. Chem. Soc.* **2017**, *139*, 4338.
(23) Escalera-Moreno, L.; Suaud, N.; Gaita-Ariño, A.; Coronado, E. *J. Phys. Chem. Lett.* **2017**, *8*, 1695.
(24) Lunghi, A.; Totti, F.; Sessoli, R.; Sanvito, S. *Nat. Commun.* **2017**, *8*, 14620.
(25) Lunghi, A.; Totti, F.; Sanvito, S.; Sessoli, R. *Chem. Sci.* **2017**, *8*, 6051.

(26) Cooper, S. R.; Koh, Y. B.; Raymond, K. N. *J. Am. Chem. Soc.* **1982**, *104*, 5092.
(27) Chi, Z.; Zhu, L.; Lu, X.; Yu, H.; Liu, B. *Z. Anorg. Allg. Chem.* **2012**, *638*, 1523.
(28) Stoll, S.; Schweiger, A. *J. Magn. Reson.* **2006**, *178*, 42.
(29) Standeley, K. J.; Vaughan, R. A. *Plenum Press, New York in 1969* **1969**, 199.
(30) Tesi, L.; Lunghi, A.; Atzori, M.; Lucaccini, E.; Sorace, L.; Totti, F.; Sessoli, R. *Dalton Trans.* **2016**, *45*, 16635.
(31) Van Vleck, J. H. *Phys. Rev.* **1940**, *57*, 426.
(32) De Vroomen, A. C.; Lijphart, E. E.; Prins, D. Y. H.; Marks, J.; Poulis, N. J. *Physica* **1972**, *61*, 241.
(33) Butcher, F. K.; Gerrard, W.; Howarth, M.; Mooney, E. F.; Willis, H. A. *AcSpe* **1964**, *20*, 79.
(34) Ponseca, C. J. S.; Estacio, E.; Murakami, H.; Sarukura, N.; Pobre, R.; Tominaga, K.; Nishizawa, J.; Sasaki, T.; Suto, K. *Journal of Physics: Conference Series* **2008**, *112*, 042073.
(35) Zheng, Z.-P.; Fan, W.-H.; Yan, H. *Chem. Phys. Lett.* **2012**, *525*, 140.
(36) Eaton, S. S.; Eaton, G. R. In *Distance Measurements in Biological Systems by EPR*; Berliner, L. J., Eaton, G. R., Eaton, S. S., Eds.; Springer US: Boston, MA, 2002, p 29.
(37) Yu, C.-J.; Graham, M. J.; Zadrozny, J. M.; Niklas, J.; Krzyaniak, M. D.; Wasielewski, M. R.; Poluektov, O. G.; Freedman, D. E. *J. Am. Chem. Soc.* **2016**, *138*, 14678.
(38) Sheldrick, G. M. **1996**.
(39) Farrugia, L. *J. Appl. Crystallogr.* **1999**, *32*, 837.
(40) Macrae, C. F.; Edgington, P. R.; McCabe, P.; Pidcock, E.; Shields, G. P.; Taylor, R.; Towler, M.; van de Streek, J. *J. Appl. Crystallogr.* **2006**, *39*, 453.
(41) Bain, G. A.; Berry, J. F. *J. Chem. Educ.* **2008**, *85*, 532.
(42) Taschin, A.; Bartolini, P.; Tasseva, J.; Torre, R. *Measurement* **2017**, DOI: 10.1016/j.measurement.2017.05.074.

TOC